Korean J. Chem. Eng., 35(4), 1009-1018 (2018)
DOI: 10.1007/s11814-017-0286-8

pISSN: 0256-1115
eISSN: 1975-7220

Change of band-gap position of $MTiO_2$ particle doped with 3d-transition metal and control of product selectivity on carbon dioxide photoreduction

Jeong Yeon Do*, Junyeong Kim*, Yeju Jang*, Youn-Kyoung Baek, and Misook Kang*,†**

*Department of Chemistry, College of Natural Sciences, Yeungnam University, Gyeongsan, Gyeongbuk 38541, Korea
**Powder & Ceramics Division, Korea Institute of Materials Science, Changwon 51508, Korea
(*Received 3 July 2017 • accepted 11 October 2017*)

Abstract−This study attempted to obtain various products from carbon dioxide photoreduction using TiO_2 catalysts doped with different transition metals of Mn, Fe, Co, Ni, Cu, and Zn ($MTiO_2$). The band-gaps of $MTiO_2$ catalysts decreased compared to pure TiO_2, except for $ZnTiO_2$. The intensities in photoluminescence curves, which can predict the recombination of excited electrons and holes, were weaker in $MTiO_2$ catalysts than that of pure TiO_2. The products obtained from carbon dioxide photoreduction were strongly related to the redox potential of carbon dioxide and the locations of band-gaps of $MTiO_2$ catalysts. Methane was predominantly obtained in pure TiO_2, $FeTiO_2$, and $NiTiO_2$ catalysts, and methanol and carbon monoxide were selectively produced in the $CuTiO_2$ and $ZnTiO_2$ catalysts, respectively. This result suggests that the desired product from carbon dioxide photoreduction can be selectively synthesized by doping certain metals.

Keywords: $MTiO_2$, 3d-Transition Metal, Carbon Dioxide Photoreduction, Methane, Carbon Monoxide, Methanol

INTRODUCTION

National efforts to reduce carbon dioxide (CO_2) emissions, which are recognized as the main cause of global warming, have been made by the United Nations Framework Convention on Climate Change (UNFCCC) in 1992 and have been formulated through the implementation of the Kyoto Protocol. Carbon capture and storage (CCS) [1], which captures and stores CO_2, and carbon capture and utilization (CCU) [2], which converts CO_2 into high value-added materials, are among the technologies being studied worldwide for reducing CO_2. The Global Agenda Councils (GAC) at the 2013 World Economic Forum in Davos, Switzerland, selected one of the ten technologies that will convert CO_2 into fuels that will have an important impact on human beings. In particular, the photochemical reduction of CO_2 in CCU technology is the most ideal and environmentally friendly technology, and has attracted many researchers in recent years.

For the photochemical reduction of CO_2, many scientists have been using semiconductor materials such as titanium dioxide (TiO_2), which have a good redox potential between CO_2 and the reduced product [3,4]. Possible reactions involved in the photocatalytic reduction of CO_2 with water (H_2O) on TiO_2 and thermodynamic redox potentials of various compounds are listed as follows [5,6].

$$TiO_2+h\nu \rightarrow e^- + h^+ \quad (1)$$

$$2\,H_2O+4\,h^+ \rightarrow 4\,H^+ + O_2,\ E^0=H_2O/O_2=+0.82\ V \quad (2)$$

$$CO_2+8\,e^- +8\,H^+ \rightarrow CH_4+H_2O,\ E^0=CO_2/CH_4=-0.24\ V \quad (3)$$

$$CO_2+6\,e^- +6\,H^+ \rightarrow CH_3OH+H_2O,\ E^0=CO_2/CH_3OH=-0.38\ V \quad (4)$$

$$2\,H^+ +4\,e^- \rightarrow H_2,\ E^0=H^+/H_2=-0.41\ V \quad (5)$$

$$CO_2+4\,e^- +4\,H^+ \rightarrow HCHO+H_2O,\ E^0=CO_2/HCHO=-0.48\ V \quad (6)$$

$$CO_2+2\,e^- +2\,H^+ \rightarrow CO+H_2O,\ E^0=CO_2/CO=-0.53\ V \quad (7)$$

$$CO_2+2\,e^- +2\,H^+ \rightarrow HCOOH,\ E^0=O_2/HCOOH=-0.61\ V \quad (8)$$

$$CO_2+e^- \rightarrow CO_2^-,\ E^0=CO_2/CO_2^-=-1.9\ V \quad (9)$$

CO_2 photoreduction with H_2O can be separated to two reactions, CO_2 reduction and H_2O oxidation. The mechanism can be simply described in the following sub-steps: (Eq. (1)) photo-illumination on the surface of photocatalyst induces the generation of charge carriers, i.e., electron-hole (e^-/h^+) pairs, (Eqs. (3), (4), (6), (7), (8), and (9)) the excited electrons in the conduction band (CB) of photocatalyst migrate to the surface and reduce CO_2 into fuels [e.g., carbon monoxide (CO), methane (CH_4), methanol (CH_3OH), formaldehyde (HCHO), and formic acid (HCOOH)], and (Eq. (5)) the holes left in the valence band (VB) of the photocatalyst oxidize H_2O into oxygen.

However, pure TiO_2 has a serious limitation for CO_2 photoreduction: the fast charge recombination rate in TiO_2 causes poor photocatalytic performance [7,8]. To solve the problem, various attempts in synthesis and surface modifications of TiO_2 catalysts have been considered as follows. First, the surface defects of TiO_2 can change its surface properties, resulting in different adsorption and desorption capabilities of reactants, intermediates, and products [9,10]. Second, light adsorption ability of TiO_2 is closely related to the band gap structure: with a reduced band gap or addition of sub-bands, TiO_2 can respond to visible light, increasing light adsorption efficiency [11,12]. Third, disorders at the surface or subsurface of TiO_2 could become traps for electrons or holes, suppressing the recom-

†To whom correspondence should be addressed.
E-mail: mskang@ynu.ac.kr

bination of electrons and holes and thus facilitating their separation [13,14]. For these attempts, in particular, doping is one of the frequently used methods to narrow down or introducing impurity levels inside the band gap of TiO_2, and possibly to improve the separation of charge carriers. Various metal [15-17] or nonmetal [18-20] elements are used as dopants. As for TiO_2, dopants could substitute the original Ti or O atom, or be placed at the interstitial position depending on the valence, radius, and electronic properties of the dopants.

So far, many studies have been carried out to increase the activity of catalysts by using dopants. However, there have been few studies to control the products produced during photoreaction using dopants. We investigated the product distributions in the CO_2 photoreduction reaction and the selectivity of the products according to the dopant species. Many papers have attempted to find a dopant with excellent photoactivity by limiting the reduction target to CH_4 [21,22]. However, we tried to determine which of the various reduction products are advantageously produced by using a metal as a dopant. For this purpose, we used 3d-transition metals (Mn, Fe, Co, Ni, Cu, and Zn) with five or more electrons as dopants, and the amount of 5.0 mol-% was inserted into the TiO_2 framework to control the band-gap of TiO_2 to improve the photoactivity by lowering the recombination rate between electrons and holes. The synthesized 5.0 mol-% 3d-Metal-TiO_2 catalysts were identified by X-ray diffraction, X-ray photoelectron spectroscopy, and transmission electron microscopy and their optical properties were characterized by UV-visible absorbance and photoluminescence measurements.

EXPERIMENTAL

1. Preparation and Characterization of 5.0 mol-% 3d-Metal-TiO_2 Particles

The pure TiO_2 and $MTiO_2$ particles (5.0 mol-% 3d-Metal-TiO_2) which inserted by 3d-transition metals of 5.0 mol-% (3d-transition metals=Mn, Fe, Co, Ni, Cu, and Zn) were prepared by a conventional sol-gel treatment as follows [23]. The amount of doped metal was limited to 5.0 mol-%, which is the optimal condition for the best catalytic performance in the previously published paper. [14]. Each metal (II) chloride ($MnCl_2{\cdot}nH_2O$, $FeCl_2{\cdot}nH_2O$, $CoCl_2{\cdot}nH_2O$, $NiCl_2{\cdot}nH_2O$, $CuCl_2{\cdot}nH_2O$, and $ZnCl_2{\cdot}nH_2O$; 99.99%, Junsei Chem. Co., Japan) having oxidation state divalent and titanium tetraisopropoxide (TTIP, 99.95%, Junsei Chem. Co., Japan) were added into the absolute ethanol solvent of 1.0 L as the metal and Ti precursors, respectively. Here, the number of moles of inserting metals corresponds to 0.05 M against to TTIP of 1.0 M. Distilled water of 6.0 M was slowly dropped into the solution so that it was six-times the number of 1.0 M of TTIP to induce $Ti(OH)_6$ in the hydrolysis stage. Acetic acid, as a homogeneous acidic catalyst to promote the condensation reaction between intermolecular $Ti(OH)_6$, was added to adjust pH=3, and the solutions were then homogeneously stirred for 2 h at room temperature. The powders of amorphous TiO_2 or $MTiO_2$ were obtained after passing through the $(\text{-Ti-O-Ti-})_n$ or $(\text{-Ti-O-M-})_n$ oligomers by a step-wise reaction following by evaporation at 70 °C over 4 h, and then the resulting powders were thermally treated at 500 °C for 5 h in an electric furnace under the air condition for crystal formation, and finally afforded to crystalline TiO_2 or $MTiO_2$. Eventually, seven catalysts--5.0 mol-% $MnTiO_2$, 5.0 mol-% $FeTiO_2$, 5.0 mol-% $CoTiO_2$, 5.0 mol-% $NiTiO_2$, 5.0 mol-% $CuTiO_2$, and 5.0 mol-% $ZnTiO_2$--were synthesized in this study. These are simplified and named as TiO_2, $MnTiO_2$, $FeTiO_2$, $CoTiO_2$, $NiTiO_2$, $CuTiO_2$, and $ZnTiO_2$.

The structures and morphologies synthesized TiO_2 and $MTiO_2$ particles were identified by X-ray diffraction (XRD, MPD, PANalytical) with nickel-filtered Cu-Kα radiation (30 kV, 30 mA) and transmission electron microscopy (TEM, H-7600, Hitachi), and the amount of atoms present on the particle surface and the oxidation states of the inserted metals were characterized by energy-dispersive spectrometry with element mapping (EDS/mapping, EX-250, Horiba) and X-ray photoelectron spectroscopy (XPS, AXIS Nova, Kratos Inc.). Optical properties of the synthesized particles were confirmed by diffuse-reflectance ultraviolet-visible spectra (UV-vis, Cary 500 spectrometer, range of 200-800 nm) and photoluminescence spectroscopy (PL, Perkin Elmer, He-Cd laser source, wavelength of 300 nm).

2. Evaluation of Catalytic Performance for Carbon Dioxide Photoreduction over 5.0 mol-% 3d-Metal-TiO_2 Particles

The CO_2 photoreduction activities on the synthesized TiO_2 and $MTiO_2$ particles with H_2O were carried out in a closed quartz vessel (length of 7.50 cm, width of 1.04 cm, and total volume of 7.00 cm^3). A schematic diagram of the photoreactor was already well documented in the previous paper [24]. 0.2 g of catalyst and 11.30 mg of distilled water were taken in the photoreactor. Supercritical fluid-grade CO_2 gas was used as reactant, and the CO_2 gas flowed into the chamber for a while to pull air out before irradiation. Then, the reactor chamber was closed and the lamp was switched on. A UV-lamp (6 Wcm^{-2}, 20 cm length×2.0 diameter, Shinan, Korea) with a 365 nm emitting light was used as the irradiation source. The photoreduction temperature and pressure were maintained at 303 K and 1.0 atm, respectively. The emitted gas products were analyzed by gas chromatography (iGC7200, DS Science, Korea) equipped with thermal conductivity (TCD) and flame ionized detectors (FID) to separate the C_1-C_3 light hydrocarbons and oxygenated compounds, such as CH_4, CH_3OH, HCOOH, and CO. The selectivity of the product was calculated using the following equation: C_i (%)=C_i moles in product/total moles of C produced ×100%.

RESULTS AND DISCUSSION

1. Physicochemical Properties of the Synthesized 5.0 mol-% 3d-Metal-TiO_2 Particles

Fig. 1 shows the XRD patterns of the TiO_2 and $MTiO_2$ particles. The XRD spectrum of pure TiO_2 and $MTiO_2$ showed peaks at 2θ values=25.3°(101), 38.0°(004), 48.2°(200), 54.0°(105), 63°(211), and 68.0°(204), assigned to the tetragonal-phase anatase structure [25]. The broad peaks indicate that the crystallite size is small. As compared with the peak of pure TiO_2, the peak width of the $MTiO_2$ was widened by the metal insertion, with reference to the main peak 101 plane. This result implies that the size of the $MTiO_2$ particles inserted with 3d-metal is smaller: The sizes of the crystallites calculated by the Scherrer equation [26] were 24.28, 21.27, 14.92, 19.34, 13.95, 18.09 and 16.68 nm in the TiO_2, $MnTiO_2$, $FeTiO_2$,

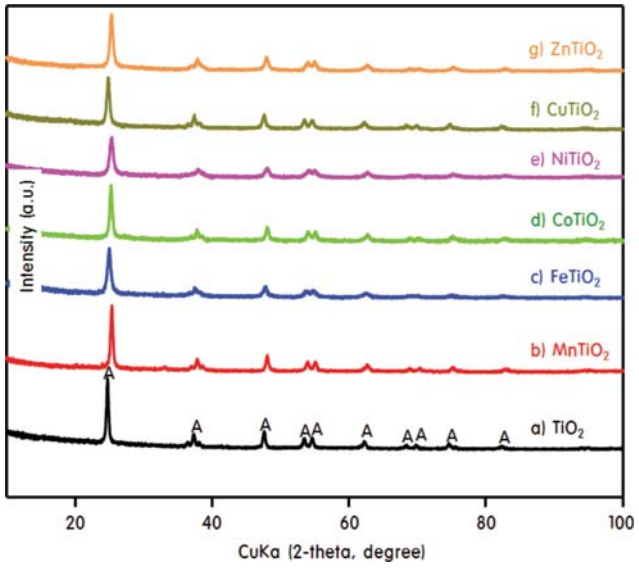

Fig. 1. XRD patterns of TiO_2 and 5.0 mol-% 3d-$MTiO_2$ particles.

$CoTiO_2$, $NiTiO_2$, $CuTiO_2$, and $ZnTiO_2$ samples, respectively. Also, the positions of the peaks were slightly shifted to higher angles. This result is probably due to the fact that the lattice distance is somewhat distorted by metal insertion. However, no metal oxide peak for the inserted 3d-metal was observed in any sample, suggesting that 5.0 mol-% of the metals were stably inserted into the TiO_2 framework.

The TEM images of for the TiO_2 and $MTiO_2$ samples, in Fig. 2, show spherical and angled typed-nanoparticles with a size of less than 30 nm except for pure TiO_2. The particle sizes of the pure TiO_2 samples were 44.9 nm, and followed by $CuTiO_2$ (27.5 nm), $CoTiO_2$ (27.4 nm) and $MnTiO_2$ (24.0 nm), respectively. In $NiTiO_2$ and $FeTiO_2$ samples, the smallest particles of sizes of 17.2 and 9.13 nm were identified, respectively. These observations are in good agreement with the XRD data.

The oxidation states of the doped metal components, Mn2p, Fe2p, Co2p, Ni2p, Cu2p, and Zn2p, into TiO_2 and $MTiO_2$ particles were quantitatively analyzed by XPS, as shown in the typical survey and high-resolution spectra in Fig. 3. First, the $2p_{1/2}$ (low-

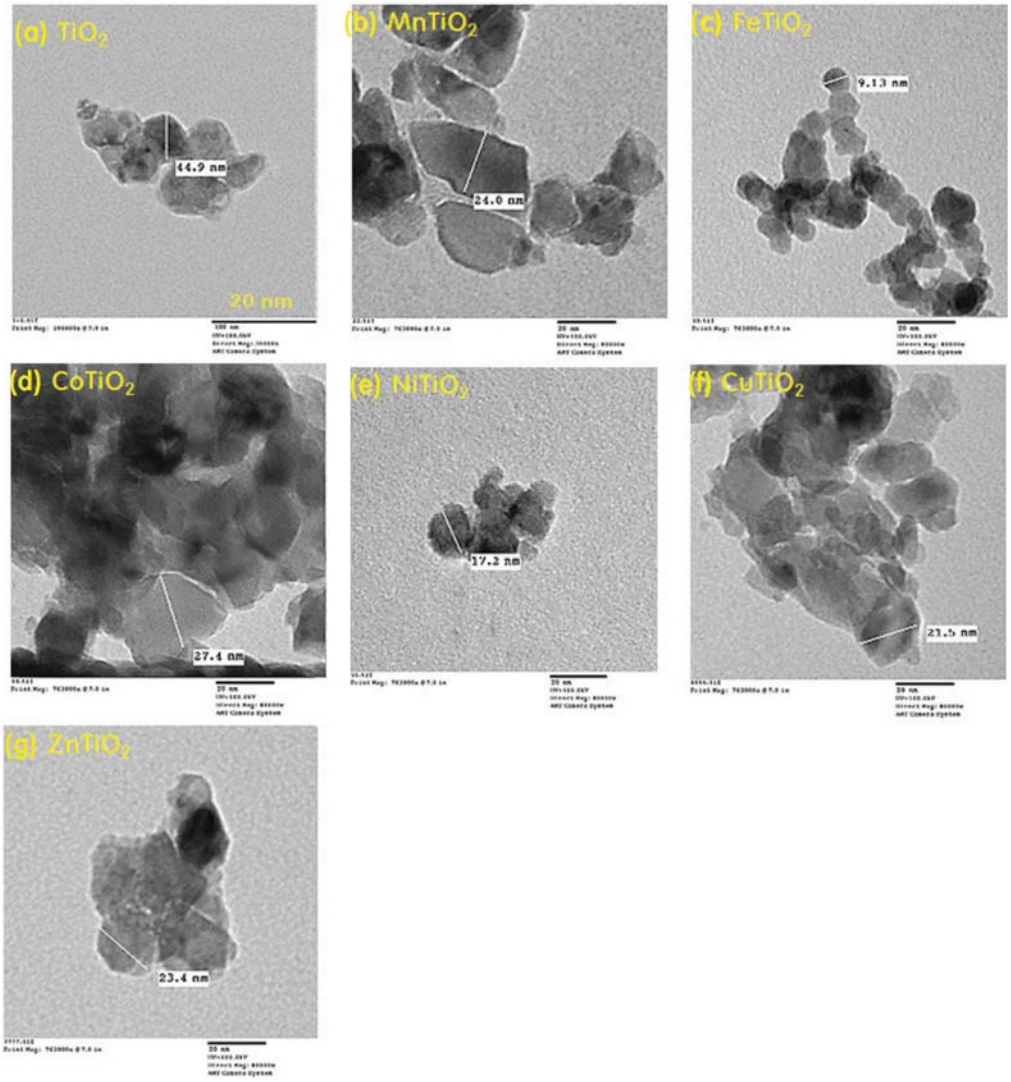

Fig. 2. TEM images of TiO_2 and 5.0 mol-% 3d-$MTiO_2$ particles.

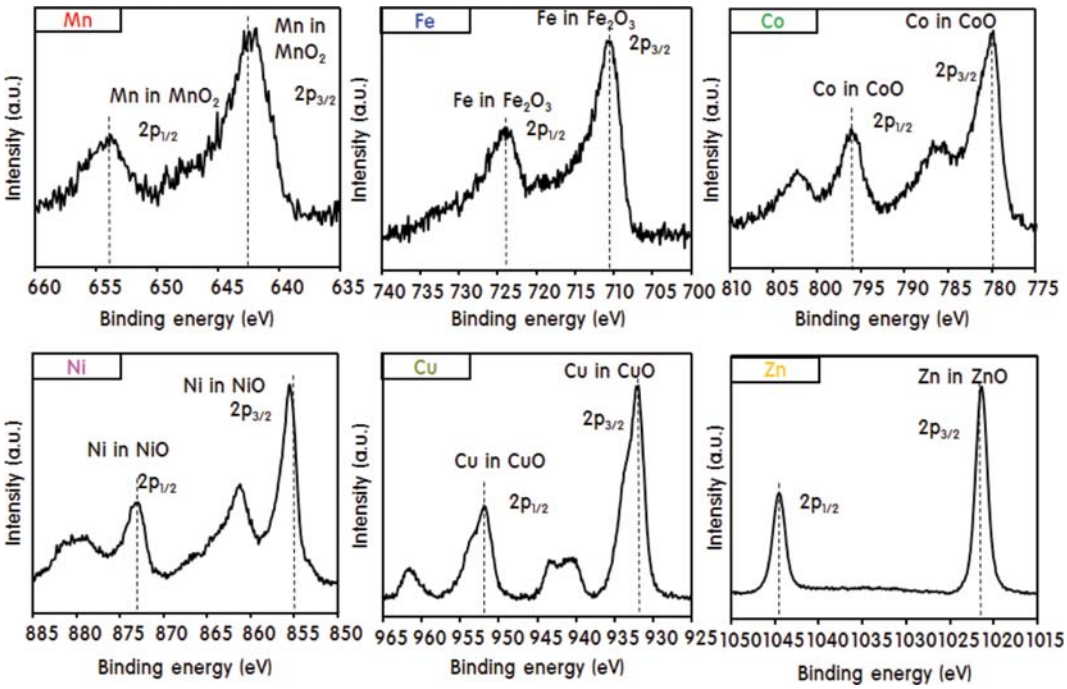

Fig. 3. High-resolution XPS spectra for Mn2p, Fe2p, Co2p, Ni2p, Cu2p, and Zn2p in 5.0 mol-% 3d-$MTiO_2$ particles.

est occupied molecular orbital) and $2p_{3/2}$ (highest occupied molecular orbital) binding energies of the Mn element in $MnTiO_2$ were clearly separated at 654.1 and 642.5 eV, assigned to MnO_2 rather than MnO [27]. The $Fe2p_{3/2}$ and $Co2p_{3/2}$ peaks in $FeTiO_2$ and $CoTiO_2$ samples were located at 710.9 and 780.0 eV, corresponding to Fe_2O_3 and CoO [28,29]. In the case of $NiTiO_2$ and $CoTiO_2$ samples, the $Ni2p_{3/2}$ and $Cu2p_{3/2}$ peaks were exhibited at 854.9 and 932.5 eV binding energies, predicted as NiO and CuO [30,31].

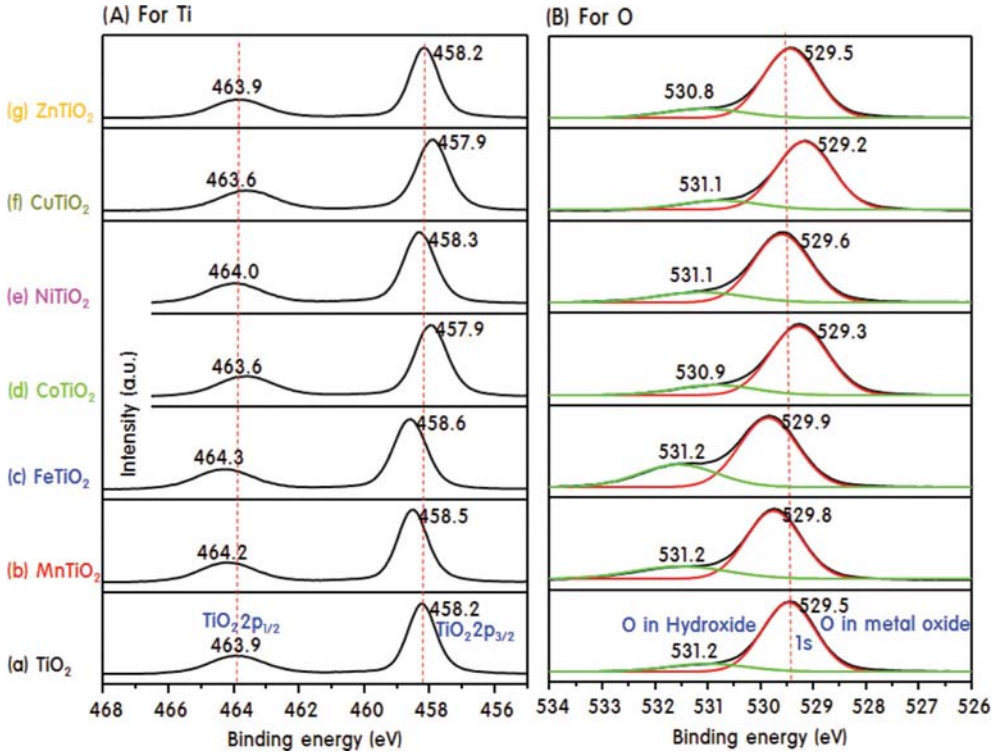

Fig. 4. XPS curves of Ti2p and O1s in TiO_2 and 5.0 mol-% 3d-$MTiO_2$ particles.

Finally, the $Znp_{1/2}$ and $Znp_{3/2}$ peaks at binding energies of 1,044.8 and 1,021.8 eV were assigned to ZnO in $ZnTiO_2$ sample [32]. From these results, we are convinced that all the inserted metals were stably present as metal oxides, and that the inserted amount was quite reliable.

XPS results of Ti and O in each sample are shown in Fig. 4 to investigate the oxidation state and the environmental change of TiO_2, the main catalyst when 3d-metals were added. The binding energy of the two elements, $Ti2p_{3/2}$ and O1s were present at 458.2 and 529.5 eV in pure TiO_2, and these peak locations were assigned to a classical Ti^{4+} and O^{2-} of TiO_2 [33]. This means that the oxidation state of titanium changed to a more oxidized state by the doping Mn, Fe, Ni, and Zn metals. However, the Ti oxidation state in the $CoTiO_2$ and $CuTiO_2$ samples could be predicted to shift to a lower oxidation state than Ti^{4+} of pure TiO_2, since the peak position shifts toward lower binding energy. On the other hand, in all samples, peaks that suggested to O1s of OH are seen near about 531 eV, which is further increased in samples with 3d-metals added compared to it of pure TiO_2. In particular, the peak area of the $FeTiO_2$ sample was the largest: in general, O1s of OH is a peak for evaluating the hydrophilicity [34]. It is known that the better the surface hydrophilicity of the catalyst, the easier the formation of

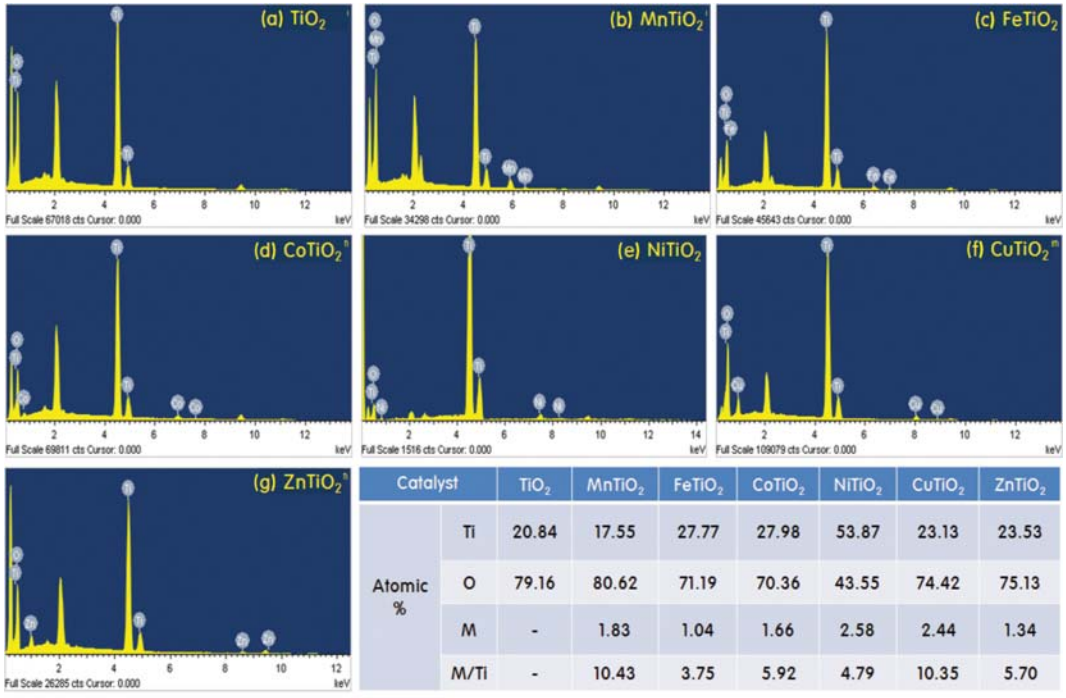

Catalyst		TiO_2	$MnTiO_2$	$FeTiO_2$	$CoTiO_2$	$NiTiO_2$	$CuTiO_2$	$ZnTiO_2$
Atomic %	Ti	20.84	17.55	27.77	27.98	53.87	23.13	23.53
	O	79.16	80.62	71.19	70.36	43.55	74.42	75.13
	M	-	1.83	1.04	1.66	2.58	2.44	1.34
	M/Ti	-	10.43	3.75	5.92	4.79	10.35	5.70

(A)

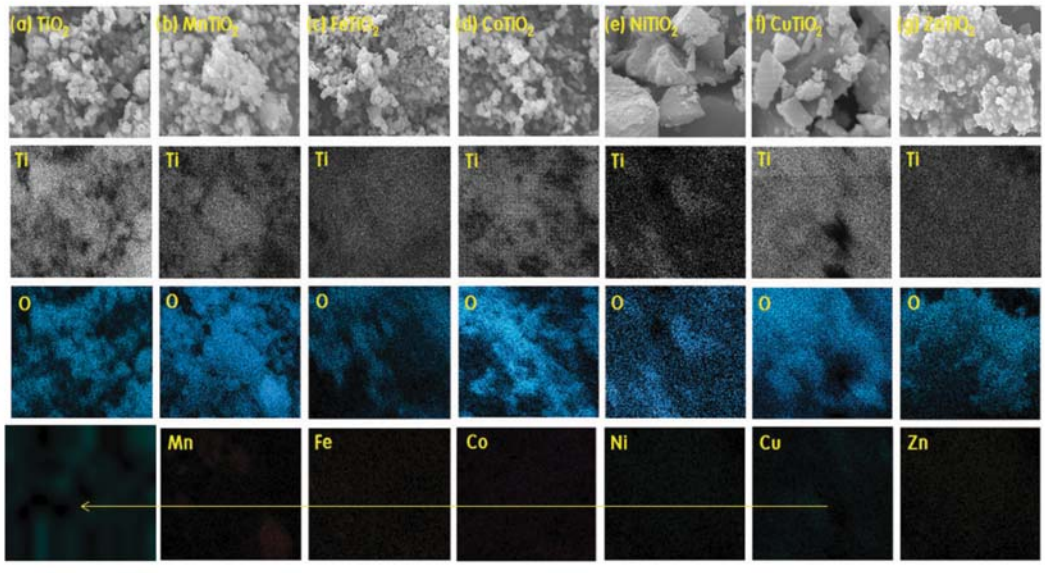

(B)

Fig. 5. EDS spectra of TiO_2 and 5.0 mol-% 3d-$MTiO_2$ particles and the metal atomic compositions.

·OH radicals during the reaction, thereby increasing the catalyst performance. Although this fact is favorable for the photooxidation reaction, the photodecomposition reaction is not yet conclusive.

Energy dispersive X-ray spectroscopy (EDS) was used to semi-quantitatively analyze the elemental composition of the surfaces on TiO_2 and $MTiO_2$ particles, and the results are shown in Fig. 5(A). The EDS analysis revealed the presence of inserted 3d-metals in $MTiO_2$, and it was confirmed that all of the elements, Mn, Fe, Co, Ni, Cu, and Zn, were inserted stably and uniformly to TiO_2 framework. The ratio of Ti : O in pure TiO_2 was about 1 : 4, which shows a higher oxygen content than the theoretical value of Ti : O= 1 : 2. This result is probably due to the fact that EDS is a device favorable for surface element analysis rather than whole element analysis. Nevertheless, the TiO_2 particles synthesized in this study are expected to have a large amount of oxygen exposed on the surface. Meanwhile, the M/Ti atomic ratios (%) were 10.43, 3.75, 5.90, 4.79, 10.55, and 5.70% in $MnTiO_2$, $FeTiO_2$, $CoTiO_2$, $NiTiO_2$, $CuTiO_2$, and $ZnTiO_2$, respectively. These values are close to the stoichiometric mole fractions of M/Ti=5.0 mol-% except of those in $MnTiO_2$ and $CuTiO_2$, having a mole fractions of M/Ti=10.0 mol-%. This result was also consistent with the EDS element mapping image results of Ti and O in Fig. 5(B). In general, the image means that the spots are the constituent atoms and the color intensity is proportional to their concentration. No aggregations between particles were observed in all catalysts. All of elements were well dispersed on the surface of catalyst particles. Furthermore, the images show the 3d-metal elements homogeneous distribution with many spaces. The mapping results for 3d-metals clearly show images with a large number of voids in comparison to that of Ti and O, maybe due to the small amount 3d-metals loaded on the surface of TiO_2. Moreover, the spots show the element percentages of 3d-metals nearly match well with the stoichiometric proportion of $MTiO_2$. From this result, we could expect that perhaps the doped metals are atomically dispersed.

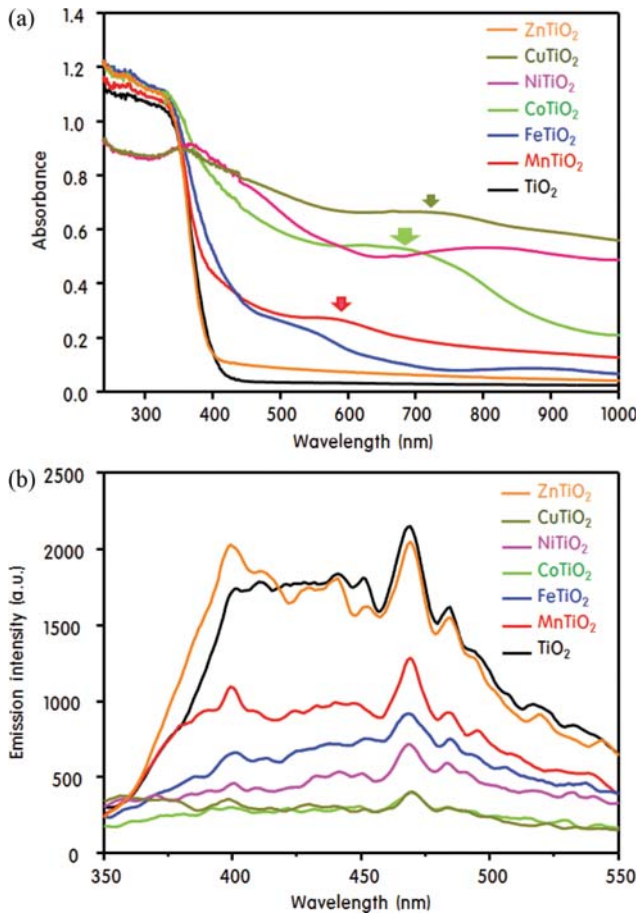

Fig. 6. UV-visible absorption (a) and PL spectra (b) of TiO_2 and 5.0 mol-% 3d-$MTiO_2$ powders.

Fig. 6 shows the UV-visible absorption spectra (a) and PL spectra (b) of the prepared TiO_2 and $MTiO_2$ powders. Generally, the band-gaps of semiconductor materials are closely related to the range of wavelengths absorbed: the higher the absorption wavelength, the shorter the band-gap [35]. In Fig. 6(a), an absorption band of anatase structured pure TiO_2 (402.9 nm) is clearly observed near 400 nm after extrapolation, which is similar to the absorption wavelength reported elsewhere [36]. The absorption curve of $ZnTiO_2$ (386.3 nm) was exhibited at the similar position with TiO_2. But, the broad absorptions were observed in another $MTiO_2$ samples; the absorptions were split into two curves: the first peak is the curve corresponding to the TiO_2 absorption and the second curve corresponds to the specific absorption of the added metals. In particular, the curves corresponding to the TiO_2 absorption shifted to larger wavelengths by the addition of metals; however, the degree of movement varied depending on the species of metal. The maximum in first curves was observed at 384, 466, 456, 590, and 594 nm in $MnTiO_2$, $FeTiO_2$, $CoTiO_2$, $NiTiO_2$, and $CuTiO_2$, respectively, and the optical band-gaps of the samples were obtained from these values as follows: 2.93, 2.47, 2.77, 1.96, 2.38, 2.04, and 3.06 eV for TiO_2, $MnTiO_2$, $FeTiO_2$, $CoTiO_2$, $NiTiO_2$, $CuTiO_2$, and $ZnTiO_2$, respectively. On the other hand, the characteristic curves for the added metals were observed at 580, 550, 670, 800 and 720 nm corresponding to the Mn^{2+}, Fe^{2+}, Co^{2+}, Ni^{2+}, and Cu^{2+} oxides, respectively. From this result, we recognized that most of the added metal was inserted into the TiO_2 framework but remained on the surface to some extent. PL measurements as shown in Fig. 6(b) are typically employed to investigate the separation efficiency of the photo-generated electron-hole pairs and charge carrier lifetime of semiconductor particles. Therefore, there is a good relationship between the PL intensity and the photo-activity. Generally, the PL intensity increases with an increase in the number of emitted electrons as a result of recombination between the excited electrons and holes and the consequent decrease in the photo-activity [37]. In this study, the samples were excited at the same wavelength of 350-550 nm corresponding to photon-energy of same ranges, and the most preferred position, around 460 nm, corresponds to blue emission. The PL spectrums of $MTiO_2$ were given and exhibited two UV emission peaks at 3.20 and 3.11 eV: two blue emission peaks at 2.82 and 2.64 eV. The strength of PL curves was strongly observed in pure TiO_2, and decreased in the order of $ZnTiO_2$, $MnTiO_2$, $FeTiO_2$, $NiTiO_2$, $CoTiO_2$, and $CuTiO_2$.

The valence band (VB) spectra were performed from XPS study of the TiO_2 and $MTiO_2$ powders to further understand the relation between electron transfer energy and CO_2 photo-reduction,

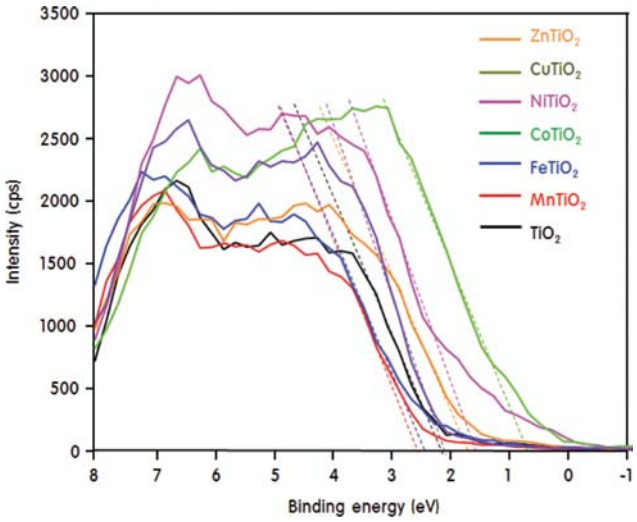

Fig. 7. Valence band spectra performed from XPS of TiO_2 and 5.0 mol-% 3d-$MTiO_2$ particles.

as shown in Fig. 7. The broad peak is identified as the valence band of the particles, and the locations of VBs of TiO_2, $MnTiO_2$, $FeTiO_2$, $CoTiO_2$, $NiTiO_2$, $CuTiO_2$, and $ZnTiO_2$ were observed at 2.20, 2.43, 2.36, 1.75, 1.61, 0.80, and 2.15 eV, respectively. These values are quite reliable, and resemble results reported in other studies [38,39]. Here, we could obtain the conduction band (CB) location energies of each catalyst by subtracting the values of band-gaps obtained in Fig. 6 with the energy positions of VB. The calculated values were −0.55, −0.04, −0.41, −0.21, −0.77, −1.24, and −0.91 eV in TiO_2, $MnTiO_2$, $FeTiO_2$, $CoTiO_2$, $NiTiO_2$, $CuTiO_2$, and $ZnTiO_2$ catalyst, respectively.

2. Catalytic Performance for Photoreduction of CO_2 over the Synthesized 5.0 mol-% 3d-Metal-TiO_2 Particles

The produced amounts for CH_4 (A), CH_3OH (B), and CO (C) gases generated during CO_2 photoreduction over TiO_2 and $MTiO_2$ catalysts are shown in Fig. 8. First, in Fig. 8(a), when comparing the catalytic activities for CH_4 production of a completely reducing substance of CO_2, a large amount of CH_4 evolved in the order of pure TiO_2<$NiTiO_2$<$FeTiO_2$ catalysts, although largely less in $CuTiO_2$ and $ZnTiO_2$ catalysts. But the CH_4 was not observed over the $MnTiO_2$ and $CoTiO_2$ catalysts; it is believed that CO_2 reduction does not occur in both catalysts. On the other hand, the amount of CH_3OH produced in the reduction products of CO_2 is shown in Fig. 8(b). As a result, it was confirmed that the greatest amount of CH_3OH is generated in the $CuTiO_2$ catalyst. In addition, the CH_3OH was also observed in $FeTiO_2$, $NiTiO_2$, TiO_2, and $ZnTiO_2$ although the amount was small, but the evolved CH_3OH amount was much smaller than the amount generated in the $CuTiO_2$ catalyst. Therefore, it was confirmed that the reduction from CO_2 to CH_3OH was advantageously performed in $CuTiO_2$ catalyst. Similar to the results of CH_4 production, CH_3OH was not observed in $MnTiO_2$ and $CoTiO_2$. Finally, the amount of CO produced as a result of the initial reduction of CO_2 is compared in Fig 8(c). The production of CO was the most abundant in $CuTiO_2$, and its amount was twice that of CH_3OH. Next, the $ZnTiO_2$ catalyst also produced a large amount of CO, which is much higher

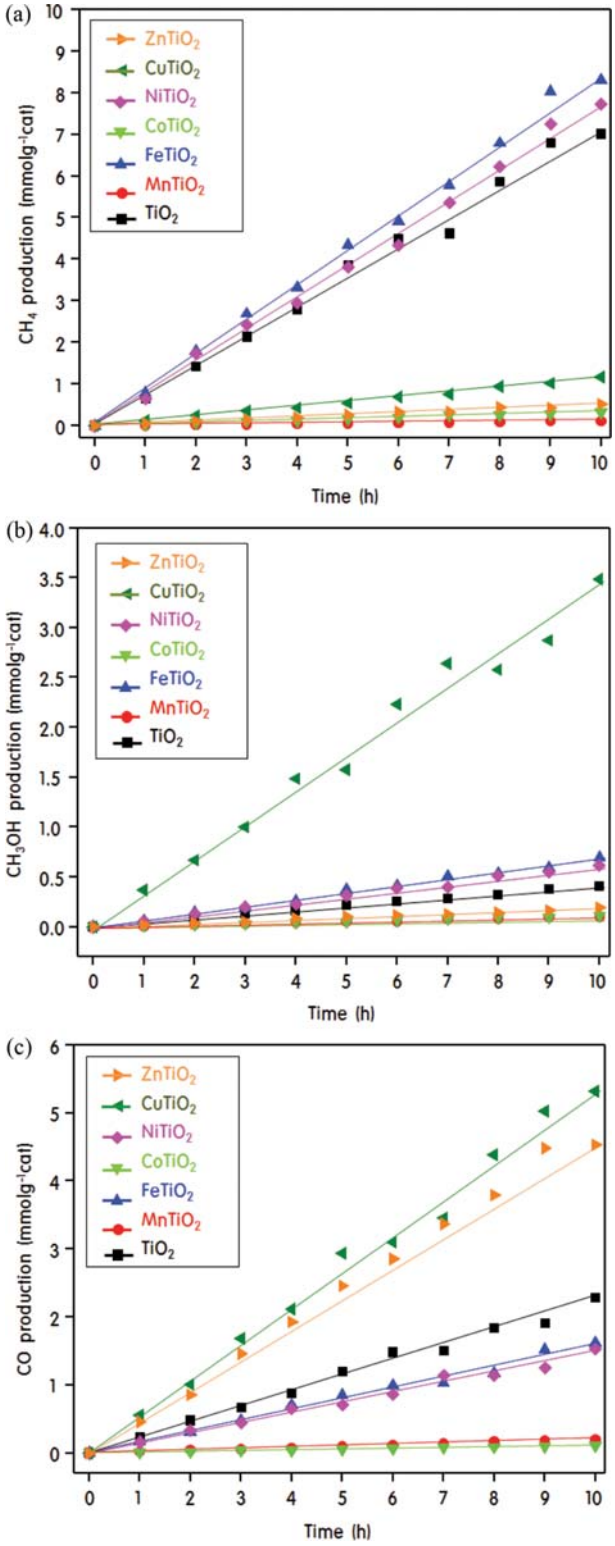

Fig. 8. CH_4 (a), CH_3OH (b), and CO (c) product distributions during CO_2 photoreduction over TiO_2 and 5.0 mol-% 3d-$MTiO_2$ catalysts.

than CH_4 and CH_3OH, suggesting that the conversion from CO_2 to CO is selectively taking place on $ZnTiO_2$. In the next order, the amounts decreased in order to pure TiO_2, $FeTiO_2$, and $NiTiO_2$ cat-

alysts, and their amounts were three-times smaller than the amount of CH_4 produced. No generation of CO was also observed in $MnTiO_2$ and $CoTiO_2$ catalysts. Eventually, the Fig. 8 results are indicating that the distribution of the reduction products of CO_2 varies depending on the doped metals, which is related to the band-gap position of the catalysts and the CO_2 redox potential.

Based on the band-gaps obtained from UV-visible absorption analysis and the VB location energies determined from XPS spectroscopic measurement, the energy potential diagrams on TiO_2 and $MTiO_2$ were predicted, and exhibited in Fig. 9(A). The CB energy location is obtained from the VB energy location minus the band gap. The most important point here is the redox potential position between carbon dioxide and the product. As shown in the figure, CO_2/CO=−0.53 V, CO_2/CH_3OH=−0.38 V, $CO_2/HCOOH$=−0.61 V, and CO_2/CH_4=−0.24 V are possible redox potentials in the CO_2 reduction reaction [40]. To obtain the desired reduction products, the energy positions of VB and CB in the catalyst should suitably contain these potentials. From this energy diagram, it is expected that the most reduction products, like CO, CH_3OH, and CH_4 except of HCOOH, will be produced in pure TiO_2. In $MnTiO_2$ and $CoTiO_2$ catalysts, the oxidation reaction will be advantageous rather than the reduction reaction, so that the reduction product

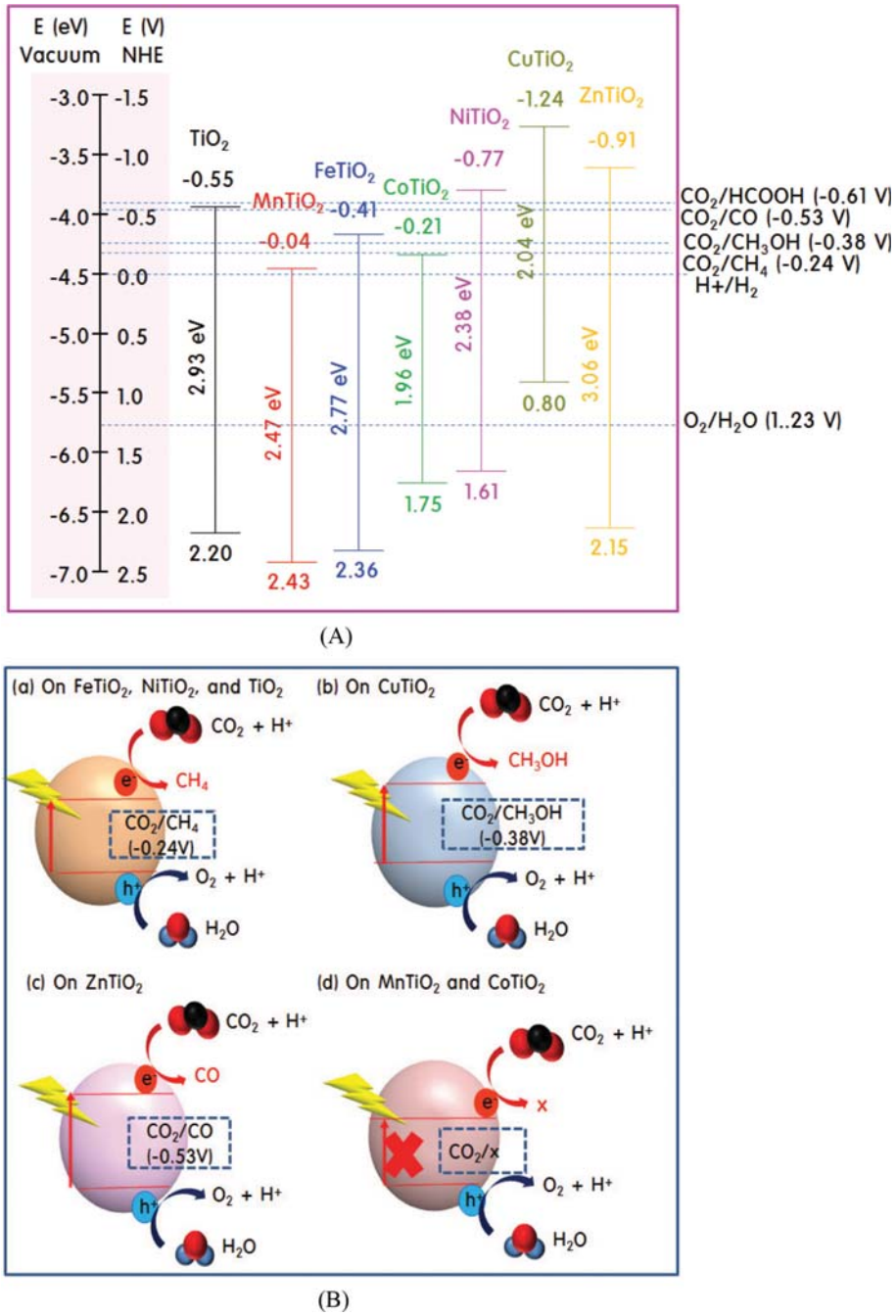

Fig. 9. Energy potential diagram (A) and expected CO_2 photoreduction mechanism (B) over TiO_2 and 5.0 mol-% 3d-$MTiO_2$ catalysts.

will not be obtained, because they do not contain a reduction potential corresponding to any reduction product. It is expected that CH_4 and CH_3OH are mainly produced in $FeTiO_2$, and all products such as HCOOH, CO, CH_3OH and CH_4 are expected in $NiTiO_2$, $CuTiO_2$, and $ZnTiO_2$. However, as expected, it was not exactly matched; in particular, there is one more thing to remember, the redox potential of water oxidation. Fortunately, most catalysts include the redox potential of water oxidation. However, $CuTiO_2$ did not include this region, but there was the CO_2 photoreduction and CH_3OH was produced. The UV-visible spectra in Fig. 6 showed the isolated CuO absorption curve in the visible region with the absorption peak of $CuTiO_2$, spontaneously. This result implies that Cu was inserted into the TiO_2 framework, but was also exposed as CuO on the surface of TiO_2. Thus, the state of the $CuTiO_2$ catalyst in this study maybe is rather closer to the mixture of $CuTiO_2$ and TiO_2/CuO. Therefore, the band energy position of the $CuTiO_2$ catalyst seems reasonable to be widely recognized from 2.20 eV of VB of TiO_2 to −1.24 eV of CB of $CuTiO_2$. For this reason, it can be deduced that a CO_2 reduction reaction occurs over $CuTiO_2$. Even though there is no guarantee, the possibilities are reasonable. On the basis of the results, we can describe the expected CO_2 photoreduction mechanisms by dividing the catalysts into four classes according to product preference as shown in Fig. 9(B). As shown, the CH_4 was selectively produced in $FeTiO_2$, $NiTiO_2$, and pure TiO_2 catalysts, and the CH_3OH was predominantly produced in $CuTiO_2$. In $ZnTiO_2$ catalyst, the CO was mainly produced, but the reduction reaction did not proceed any more. It was also found that the CO_2 reduction reactions over $MnTiO_2$ and $CoTiO_2$ catalysts were difficult to occur. This is relevant that the location energies of band-gaps for two catalysts do not include any possible redox potentials in the CO_2 reduction reactions. Their CBs are located at a higher energy level than the redox potentials for the CO_2 reduction reactions. It is therefore expected that thermodynamically reducing carbon dioxide will not occur on these catalysts. Furthermore, we could describe the CO_2 photoreduction mechanism over $MTiO_2$ catalysts as the following steps. First, by light irradiation, the surface of $MTiO_2$ photocatalyst induces the generation of charge carriers, i.e., electron-hole pairs. Then, the excited electrons on the conduction band of photocatalyst migrate to the surface and meet CO_2. Here, two possible pathways are proposed for reduction of CO_2, in particular to obtain CH_4 [41]. The one is converted to CH_4 via formaldehyde through $CO_2 \rightarrow HCOOH \rightarrow HCHO \rightarrow CH_3OH$ and finally CH_4. The other is carbon pathway, which is converted to CH_4 via $CO_2 \rightarrow CO \rightarrow C\cdot \rightarrow CH_3 \rightarrow CH_3OH$. Since HCOOH and HCHO products were not observed in this study, thus we were confident that the CO_2 reduction reaction would proceed to the carbon pathway. On the other hand, there are also two proposals for the conversion of CO_2 to CO in the initial step [42]: one is the $CO_2 \rightarrow CO_2^- \rightarrow CO$ pathway in which one electron participates and the other is the $CO_2 \rightarrow CO$ pathway in which two electrons participate. By the CO_2 redox potential value which already was commented on in the introduction section, the first and second pathways correspond to −1.90 and −0.53 V, respectively. Matching this fact with the $MTiO_2$ band-gap energy diagram results in Fig. 9(A), perhaps the second pathway in this study is more plausible. Meanwhile, the holes left in the valence band of the photocatalyst could oxidize H_2O into oxygen in final step of CO_2 photoreduction reaction.

CONCLUSIONS

A typical sol-gel method was used to prepare $MTiO_2$ nanoparticles containing 5.0 mol-% of various 3d-transition metals in the TiO_2 framework and to apply for as a catalyst for photo-reduction of CO_2. The synthesized nanoparticles were identified as an anatase structure by XRD and TEM. Their optical properties were confirmed by UV-visible absorbance and PL measurements: visible light absorptions were observed in most of the catalysts except for pure TiO_2 and $ZnTiO_2$, and the PL curves of smaller intensities were confirmed compared to TiO_2. In the CO_2 photoreduction reaction, we could predict the reduction products of CO_2 from the correlation between the redox potential of CO_2 and the position of the band-gap of the catalyst. Various reduction products were obtained depending on the contained metal components: the $FeTiO_2$ and $NiTiO_2$ catalysts including pure TiO_2 produced mainly CH_4 and about 15-30% CO, and CH_3OH was produced in a small amount compared with other products. In $CuTiO_2$ catalyst, the CO and CH_3OH (in particular it is much) were obtained as main products, and CH_4 was produced in relatively small amounts. CO gas was observed as the main product in $ZnTiO_2$. On the other hand, almost no reduction products were observed in $MnTiO_2$ and $CoTiO_2$, so that it is considered that the CO_2 reduction reaction hardly occurs. Based on CH_4 production, which is the final target of the reduction reaction, the dopants that effectively reduced CO_2 were Fe and Ni. From these results, we are convinced that changing the kind of dopant can increase the selectivity of the desired product.

ACKNOWLEDGEMENTS

This research was supported financially by the Fundamental Research Program (PNK 5450) of Korea Institute of Materials Science.

REFERENCES

1. A. Wilk, L. Więcław-Solny, A. Tatarczuk, A. Krótki, T. Spietz and T. Chwoła, *Korean J. Chem. Eng.*, **34**, 2275 (2017).
2. Z. Cui, J. Fan, H. Duan, J. Zhang, Y. Xue and Y. Tan, *Korean J. Chem. Eng.*, **34**, 29 (2017).
3. H. Huang, J. Lin, G. Zhu, Y. Weng, X. Wang, X. Fu and J. Long, *Angew. Chem. Int. Ed.*, **55**, 8314 (2016).
4. S. Xie, Q. Zhang, G. Liu and Y. Wang, *Chem. Commun.*, **52**, 35 (2016).
5. Z. He, L. Wen, D. Wang, Y. Xue, Q. Lu, C. Wu, J. Chen and S. Song, *Energy Fuel*, **3982**, 28 (2014).
6. S. Nahar, M. F. M. Zain, A. A. H. Kadhum, H. A. Hasan and M. R. Hasan, *Materials*, **629**, 10 (2017).
7. M. Zalfani, Z.-Y. Hud, W.-B. Yu, M. Mahdouani, R. Bourguiga, M. Wua, Y. Li, G. V. Tendeloo, Y. Djaoued and B.-L. Su, *Appl. Catal. B: Environ.*, **205**, 121 (2017).
8. Y. Yang, T. Zhang, L. Le, X. Ruan, P. Fang, C. Pan, R. Xiong, J. Shi

and J. Wei, *Sci. Rep.*, **4**, 7045 (2014).
9. H. Zhao, F. Pan and Y. Li, *J. Materiomics*, **3**, 17 (2017).
10. Y. Im, J. H. Lee and M. Kang, *Korean J. Chem. Eng.*, **34**(6), 1669 (2017).
11. M. Zhang, J. Wu, D. D. Lu and J. Yang, *Int. J. Photoenergy*, **2013**, 1 (2013).
12. S. Ali Ansari, M. Mansoob Khan, M. Omaish Ansari and M. H. Cho, *New J. Chem.*, **40**, 3000 (2016).
13. F. M. Pesci, G. Wang, D. R. Klug, Y. Li and A. J. Cowan, *J. Phys. Chem. C*, **117**, 25837 (2013).
14. K. Zhang and J. H. Park, *J. Phys. Chem. Lett.*, **8**, 199 (2017).
15. J. H. Lee, H. Lee and M. Kang, *Mater. Lett.*, **178**, 316 (2016).
16. M. Park, B. S. Kwak, S. W. Jo and M. Kang, *Energy Conv. Manage.*, **103**, 431 (2015).
17. D. Dvoranová, V. Brezová, M. Mazúr and M. A. Malati, *Appl. Catal. B: Environ.*, **37**, 91 (2002).
18. S. Sakthivel and H. Kisch, *ChemPhysChem*, **4**, 487 (2003).
19. K. Yang, Y. Dai, B. Huang and M.-H. Whang, *J. Phys. Chem. C.*, **113**, 2624 (2009).
20. T. Ohno, M. Akiyoshi, T. Umebayashi, K. Asai, T. Mitsui and M. Matsumura, *Appl. Catal. A: Gen.*, **265**, 115 (2004).
21. S. Protti, A. Albini and N. Serpone, *Phys. Chem. Chem. Phys.*, **16**, 19790 (2014).
22. J. Low, J. Yu and W. Ho, *J. Phys. Chem. Lett.*, **6**, 4244 (2015).
23. H. S. Kim, D. Kim, B. S. Kwak, G. B. Han, M.-H. Um and M. Kang, *Chem. Eng. J.*, **243**, 272 (2014).
24. B. S. Kwak and M. Kang, *Appl. Surf. Sci.*, **337**, 138 (2015).
25. J. Ge, Y. Ping, G. Liu, G. Qiao, E. J. Kim and M. Wang, *Mater. Lett.*, **181**, 216 (2016).
26. A. W. Burton, K. Ong, T. Rea and I. Y. Chan, *Micropor. Mesopor. Mater.*, **117**, 75 (2009).
27. G. O. Park, J. K. Shon, Y. H. Kim and J. M. Kim, *J. Nanosci. Nanotechnol.*, **15**, 2441 (2015).
28. X. Deng and C. Matranga, *J. Phys. Chem. C.*, **113**, 11104 (2009).
29. Z.-J. Jiang and Z. Jiang, *Sci. Rep.*, **6**, 27081 (2016).
30. M. Muruganandham, R. P. S. Suri, M. Sillanpää, G.-J. Lee and J. J. Wu, *Electron. Mater. Lett.*, **12**, 693 (2016).
31. F. Wu, S. Banerjee, H. Li, Y. Myung and P. Banerjee, *Langmuir*, **32**, 4485 (2016).
32. H. Tian, H. Fan, G. Dong, L. Ma and J. Ma, *RSC Adv.*, **6**, 109091 (2016).
33. J. Fang, F. Shi, J. Bu, J. Ding, S. Xu, J. Bao, Y. Ma, Z. Jiang, W. Zhang, C. Gao and W. Huang, *J. Phys. Chem. C.*, **114**, 7940 (2010).
34. S. Benkoula, O. Sublemontier, M. Patanen, C. Nicolas, F. Sirotti, A. Naitabdi, F. Gaie-Levrel, E. Antonsson, D. Aureau, F.-X. Ouf, S.-I. Wada, A. Etcheberry, K. Ueda and C. Miron, *Sci. Rep.*, **5**, 15088 (2015).
35. H. Sun, L. Biedermann and T. C. Bond, *Geophys. Res. Lett.*, **34**, 17813 (2007).
36. J. Peña-Flores, A. F Palomec-Garfias, C. Márquez-Beltrán, E. Sánchez-Mora, E. Gómez-Barojas and F. Pérez-Rodríguez, *Nanoscale Res. Lett.*, **9**, 499 (2014).
37. J. Chae and M. Kang, *J. Power Source*, **196**, 4143 (2011).
38. R. da S. Santos, G. A. Faria, C. Giles, C. A. P. Leite, H. de S. Barbosa, M. A. Z. Arruda and C. Longo, *Appl. Mater. Interf.*, **4**, 5555 (2012).
39. S. Ghasemi, S. Rahimnejad, S. Rahman Setayesh, S. Rohani and M. R. Gholami, *J. Hazard. Mater.*, **172**, 1573 (2009).
40. Y. Hori, *Modern Aspect Electrochem.*, **42**, 89 (2008).
41. J. Chen, L. Falivene, L. Caporaso, L. Cavallo and E. Y.-X. Chen, *J. Am. Chem. Soc.*, **138**, 5321 (2016).
42. S. Saeidi, N. A. Saidina Amin and M. R. Rahimpour, *J. CO_2 Utilization*, **5**, 66 (2014).